Icarus 242 (2014) 142–148

Contents lists available at ScienceDirect

Icarus

journal homepage: www.elsevier.com/locate/icarus

Phase-ratio images of the surface of Mercury: Evidence for differences in sub-resolution texture

David T. Blewett [a,*], Connor L. Levy [a,b,1], Nancy L. Chabot [a], Brett W. Denevi [a], Carolyn M. Ernst [a], Scott L. Murchie [a]

[a] Planetary Exploration Group, The Johns Hopkins University Applied Physics Laboratory, Laurel, MD 20723, USA
[b] Century High School, Sykesville, MD 21784, USA

ARTICLE INFO

Article history:
Received 21 April 2014
Revised 11 August 2014
Accepted 14 August 2014
Available online 23 August 2014

Keywords:
Mercury, surface
Geological processes
Regoliths
Image processing
Impact processes

ABSTRACT

Analysis of images that were obtained at different phase angles can give clues to the texture of a planetary surface. Here we describe *MESSENGER* phase-ratio images for features on the surface of Mercury, including hollows on the floor of Eminescu basin, a pyroclastic deposit found within the Caloris basin, and a dark impact-melt flow produced by the impact that formed Waters crater. The results indicate that hollows and the pyroclastic material are characterized by finer particle size or smoother sub-resolution roughness than the ordinary impact-generated regolith. The impact melt flow appears to have a surface that is rougher or consists of coarser particle sizes than the nearby background.

1. Introduction

The reflectance of a surface is a function of the photometric conditions, i.e., the illumination (incidence, *i*), observing (emergence, *e*), and phase (*g*) angles (e.g., Hapke, 2012). The phase angle is the angle between the directions of incidence and emergence. The manner in which the brightness of a given surface changes with phase angle is controlled by factors such as the albedo, textural properties (porosity, roughness, particle size), and scattering characteristics of the particles. Therefore, different materials may change their brightness at different rates as the phase angle changes. This phenomenon can be used to infer differences in scattering properties or sub-resolution texture from images of a planetary surface collected at different phase angles. Generally, brightness increases as phase angle decreases because of the opposition effect (see discussion by Hapke, 2012). At opposition ($g = 0$), shadows are hidden behind the objects casting them, and hence an observer sees a surface that is much brighter than the same surface observed at nonzero phase, when shadows are visible to varying degrees. The texture of the surface determines the amount of shadowing, and also influences the extent to which incident illumination is multiply scattered between surface facets or among and within regolith particles (Shkuratov et al., 2005). Multiple scattering in turn causes shadowed areas to be partially illuminated, thus affecting the reflectance of the surface as measured by a distant observer. Coherent backscatter can also contribute to the strong increase in brightness near zero phase angle (e.g., Hapke, 2002; Shkuratov et al., 2002; Kaydash et al., 2013).

Differences in phase behavior can be mapped out by co-registering two images of the same surface that were obtained at different phase angles. The ratio image formed by dividing one of the images by the other highlights features for which the phase function departs from that of the majority of the scene. Phase-ratio images have been employed to identify differences in regolith texture at a number of locations on the Moon, including the use of telescopic images (Shkuratov et al., 2010) and *Clementine* ultraviolet–visible images (Kreslavsky and Shkuratov, 2003). Images from the *Lunar Reconnaissance Orbiter* camera were used in phase-ratio studies of *Apollo*, *Luna* and *Surveyor* landing sites (Kaydash et al., 2011; Kaydash and Shkuratov, 2012, 2014; Shkuratov et al., 2013; Clegg et al., 2014) and of such other features as impact craters Kepler and Cauchy (Kaydash et al., 2012), impact melts at Giordano Bruno crater (Shkuratov et al., 2012), and haloes and rays around young craters (Kaydash et al., 2014).

Here we examine surfaces on Mercury with images returned by the Mercury Dual Imaging System (MDIS) (Hawkins et al., 2007, 2009) on the *MErcury Surface, Space ENvironment, GEochemistry, and Ranging* (*MESSENGER*) spacecraft. Of particular interest for

* Corresponding author.
E-mail address: david.blewett@jhuapl.edu (D.T. Blewett).
[1] Present address: Boston University, Boston, MA 02215, USA.

http://dx.doi.org/10.1016/j.icarus.2014.08.024
0019-1035/

Mercury are hollows (Blewett et al., 2011, 2013; Thomas et al., 2014), pyroclastic deposits (Head et al., 2008; Kerber et al., 2011; Goudge et al., 2014), and a prominent flow of dark impact melt (Klima et al., 2011; D'Incecco et al., 2013). A brief description of the features considered in this report is given in the next section.

2. Description of geologic features

2.1. Hollows

Hollows on Mercury are shallow, flat-floored, high-reflectance depressions mostly associated with impact structures (Blewett et al., 2011, 2013; Thomas et al., 2014). Some hollows are surrounded by high-reflectance haloes. Analysis of the distribution of hollows indicates that they form in low-reflectance material, one of Mercury's major color units (Robinson et al., 2008; Denevi et al., 2009). Hollows have spectral slopes at visible to near-infrared (NIR) wavelengths that are shallower ("bluer") than that of the average spectrum for Mercury's surface. The extremely fresh appearance of hollows suggests that they may be actively forming at present via a sublimation-like process related to loss of a volatile-bearing phase in the harsh thermal and space-weathering environment of Mercury's surface (Blewett et al., 2011, 2013). Hence, it would be expected that the texture and particle-size distribution of hollows could differ from that of ordinary impact-generated regolith. A striking example of hollows is presented in Fig. 1. The hollows are on the floor of Eminescu, a 120-km-diameter impact structure (centered at 10.7°N, 245.7°E) that has been morphologically categorized as a ringed peak-cluster basin (Schon et al., 2011; Baker et al., 2011).

2.2. Pyroclastic deposit

Materials that were deposited by explosive volcanic eruptions were discovered in images returned from *MESSENGER*'s first Mercury flyby in January 2008 (Head et al., 2008, 2009). Since then more than 50 examples have been cataloged (Kerber et al., 2011; Goudge et al., 2014). The deposits are generally higher in reflectance than their surroundings and have an overall spectral slope in the visible to NIR that is steeper ("redder") than that of the average spectrum for Mercury's surface (Robinson et al., 2008; Murchie et al., 2008; Blewett et al., 2009). Pyroclastic deposits are another example of surfaces that may have particle-size distributions or textures that differ from those of normal regolith. One of the most prominent examples of a pyroclastic deposit on Mercury is located in the southwestern portion of the Caloris basin, near 22°N, 146°E (Head et al., 2008, 2009). The feature consists of an irregular, rounded, rimless depression that is surrounded by a high-reflectance annular deposit with diffuse edges (Fig. 2).

2.3. Impact melt flow

A prominent tongue of low-reflectance impact melt extends ~20 km from a bright, rayed 13-km-diameter impact crater (Waters) located at ~9°S, 255°E (Fig. 3). The melt flow has a distinctive, relatively flat spectral slope (Klima et al., 2011; D'Incecco et al., 2013). The high degree of morphological freshness of the crater and the high-reflectance ray system indicate that Waters is geologically young. The combination of relative youth and the potential for lava-like cooling and flow features suggest that the surface of the impact melt could possess a texture distinct from that of typical mature soils.

3. Data

The *MESSENGER* database was searched for sets of returned MDIS images for features of interest. We sought images that have similar spatial resolutions but differences in phase angle of >~10°. It is desirable to work with images that have similar incidence angles, to minimize differences in the length and orientation of shadows and to aid in registration of the image pair. Information on the images used in this paper is given in Table 1. We utilized image pairs from either the MDIS narrow-angle camera (NAC) or

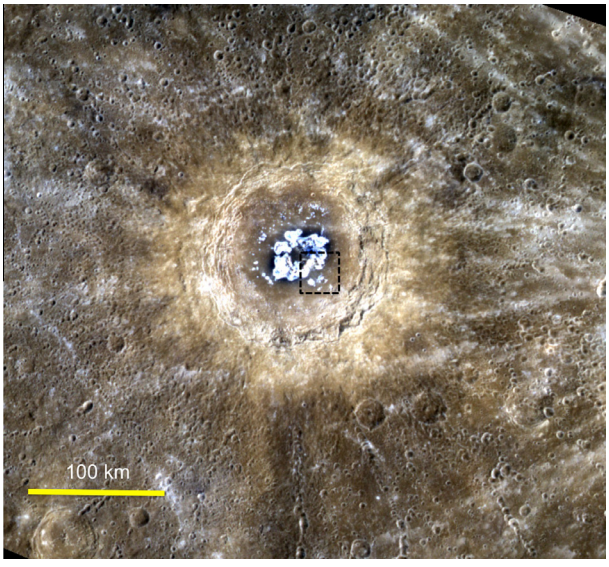

Fig. 1. Color composite image of Eminescu basin, centered near 10.7°N, 114.3°E. Dashed box shows the area of Fig. 4. Hollows on the floor and central peak cluster have characteristic high reflectance and relatively blue color. MDIS images from the 996-, 748-, and 433-nm filters displayed as red–green–blue (images EW0234069356I, EW0234069376G, EW0234069360F, 466 m/pixel). (For interpretation of the references to color in this figure legend, the reader is referred to the web version of this article.)

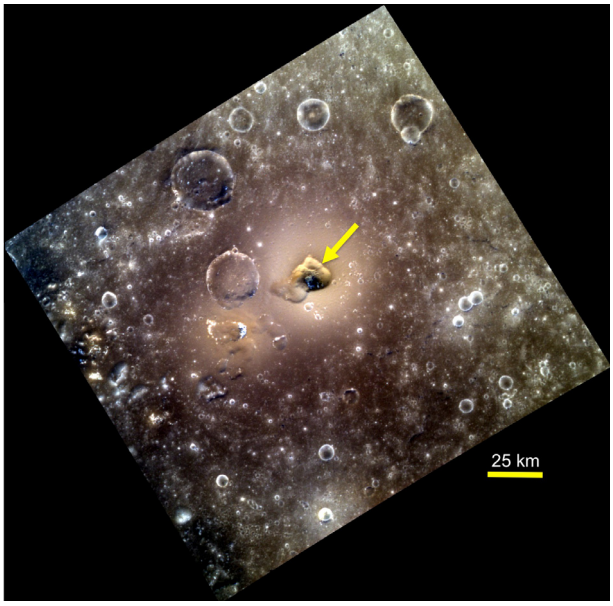

Fig. 2. Color composite image centered at 22.0 N, 146.1 E, of a volcanic vent (arrow) and surrounding pyroclastic deposit in southwestern Caloris basin. MDIS images from the 996-, 748-, and 433-nm filters displayed as red–green–blue (images EW1012859924I, EW1012859916G, EW1012859912F, 209 m/pixel). (For interpretation of the references to color in this figure legend, the reader is referred to the web version of this article.)